interesting because it allows in situ dynamic control of the spatial decay length. Thus, one can vary both ρ and σ (Eq. 7) so as to achieve values for L (either statically or dynamically) ranging from a few micrometers to 1 cm.

We have shown that this simple device, made from layers of conducting polymers, provides both logarithmic compression and lateral inhibition of response, as required for local contrast control. Nevertheless, the plastic retina is at an early stage of development. The utility of the PGT array for image enhancement will depend on a number of factors—including, for example, sensitivity, noise, dynamic range, and matching from one pixel to the next—that must be tested on an engineering prototype.

For a full plastic retina, the PGT image enhancement array would be fabricated directly onto the output side (back) of a photodetector array (for example, an infrared detector array) with each detector output pad as the anode or cathode of the PGT at that node. The semiconductor layers would be cast sequentially from solution and applied onto the detector array much like an antireflection coating. The final contrast-enhanced output would be connected to a demultiplexer by "bump bonding"; that is, by cold-welding indium bumps arrayed reciprocally on the PGT array output and on the demultiplexer input.

Alternatively, the PGT array could be used to process the image after analog-to-digital conversion and integrated directly into a display (such as a liquid-crystal display). In this case, the PGT array would be fabricated directly on, as an integral part of, the display: for example, between the control circuits and the liquid-crystal layer. The data would be logarithmically compressed digitally and input into the PGT array to process the image; the output from the pixels of the array of PGTs would serve as the input to the pixels of the display.

REFERENCES AND NOTES

1. C. Mead, *Analog VLSI and Neural Systems* (Addison-Wesley, Menlo Park, CA, 1989).
2. C. Koch and H. Li, Ed., *Vision Chips: Implementing Vision Algorithms with Analog VLSI Circuits* (IEEE Computer Society Press, Los Alamitos, CA, 1994).
3. Y. Yang and A. J. Heeger, U.S. patent application 08/227,979; *Nature* **372**, 244 (1994).
4. S. M. Sze, *Physics of Semiconductor Devices* (Wiley, New York, 1981).
5. M. Reghu *et al.*, *Phys. Rev. B* **50**, 13931 (1994).
6. I. D. Parker, *J. Appl. Phys.* **75**, 1656 (1994); G. Yu, K. Pakbaz, A. J. Heeger, *Appl. Phys. Lett.* **64**, 3422 (1994), and references therein; H. Tomozawa, D. Braun, S. D. Phillips, A. J. Heeger, *Synth. Met.* **22**, 63 (1987).
7. The images in Fig. 1 were generated with the Radiance computer graphics rendering program, developed by G. Ward and funded by the Lighting Group at Lawrence Berkeley Laboratory, U.S. Department of Energy, and the Laboratory d'Energie Solaire et de Physique du Batiment at the Ecole Polytechnique Federale de Lausanne in Switzerland.

29 June 1995; accepted 3 October 1995

Laser-Driven Movement of Three-Dimensional Microstructures Generated by Laser Rapid Prototyping

Olaf Lehmann and Michael Stuke*

Three-dimensional microstructures consisting of aluminum oxide and aluminum were fabricated by laser-induced direct-write deposition from the gas phase. Trimethylamine alane and oxygen were used as precursors. Thermal expansion forces resulting from suitable laser irradiation were used to drive the movement of microstructure parts. Applications include micromechanical actuators, such as microtweezers and micromotors. The one-step nature of the laser direct-write process allows rapid prototyping of such devices.

Lithography and etching techniques that were originally developed for microelectronics applications can also be used to fabricate sensors, actuators, or other micromechanical devices on silicon. However, these techniques require photo masks to be made before the microstructures can be produced, and the production itself consists of many complicated and time-consuming steps—for example, because vertical structure variations can be performed only indirectly. Structural redevelopment often requires redesign of the masks. As a result, such techniques are economical mainly for mass production of devices that do not need any further development. Other mask-based techniques, such as the x-ray deep etching technique LIGA (Lithographie, Galvanoformung, Abformung), also suffer from this drawback.

As a result, methods for the single-step generation of three-dimensional (3D) microstructures have recently received considerable attention. The idea is to design a structure with the use of computer-aided technologies and to transfer the data directly to a machine, which then automatically generates a solid structure. This so-called rapid prototyping enables very fast evolution of structures, particularly when laser direct writing is used as a processing tool. Techniques based on photopolymerization or powder sintering have already been used in rapid prototyping of commercial products, but they offer only submillimeter resolution. Another possibility is fast layer-by-layer laser etching of silicon in chlorine, which can be performed with a resolution of 1 μm (*1*).

Laser-assisted chemical vapor deposition (LCVD) has been shown to be suitable for rapid prototyping with micrometer resolution (*2*). The method enables fabrication of thin rods and fibers by pulling the substrate away from the stationary laser focus at a speed equal to the linear growth speed of the material, keeping the laser focus on the rod tip (*3*). LCVD was first demonstrated for carbon (*4*) and silicon (*5*) rods, but it has also been applied to the production of long carbon (*6*), silicon (*7*), and boron (*8*) fibers. More complex structures such as microsprings (*9*) have been obtained by moving the substrate on a bent track with the use of a goniometer, instead of simply pulling it linearly. Recently, we used two intersecting laser beams to create complex 3D microstructures consisting of aluminum oxide rods (*10*); our technique enables direct writing in free space in virtually any direction, as explained below.

When only one laser beam is used, LCVD can only create rods parallel or nearly parallel to the incident beam. To obtain rods in any direction, it was necessary to modify the technique. In weakly absorbing materials such as alumina, the absorption length of the laser light is large; the resulting uniform temperature distribution in the illuminated region leads to nondirectional material depo-

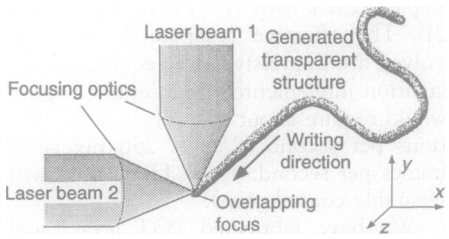

Fig. 1. Three-dimensional direct-write principle. The nearly transparent alumina rod absorbs the laser light only weakly, and thus most of the energy is absorbed in the bulk rather than at the surface. The laser beams are attenuated so that almost no growth is observable for either beam alone. The temperature rise causes nondirectional alumina deposition from the gas phase only in the area of overlapping focus, where the temperature threshold is exceeded. The writing direction is defined by slow ($\sim$10 μm s^{-1}) movement of the laser focus.

Max-Planck-Institut für Biophysikalische Chemie, P.O. Box 2841, D-37018 Göttingen, Germany.

*To whom correspondence should be addressed.

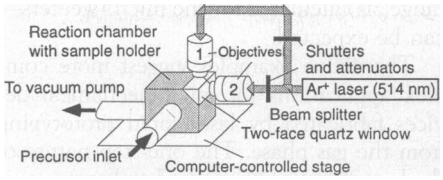

Fig. 2. Experimental setup. The reaction chamber has two tubular connections for precursor supply and pump-out, respectively. It is fixed on a computerized scanning table that can also be controlled manually by a joystick. The structure and the substrate surface are mounted inside the chamber and can be inspected with an optical microscope through a two-faced quartz window. A second objective lens allows observation from the side at a 90° angle. The laser beam, emitted from an argon ion laser (Spectra Physics 2030) working at 488 or 514 nm, is attenuated, split into two separate beams, and, after passing two computer-controlled mechanical shutters, focused through the two microscope objective lenses (magnification ×8, numerical aperture 0.2). The focal spots (diameter, ~3 μm) are adjusted to overlap, which defines the reaction zone. The shutters enable selection of one or both laser beams.

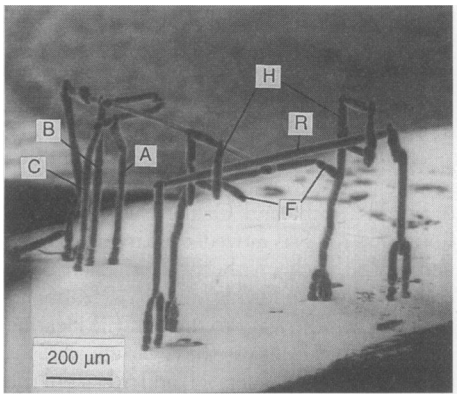

Fig. 4. Electron micrograph of the linear micromotor. The driving unit, consisting of three expandable rods (A, B, and C), is located at the back left. In the foreground, two square-ring holders (H), the horizontal movable rod (R), here still fixed to the substrate after fabrication and the fork (F) connected to the driving unit can be discerned.

sition from the gas phase around the laser spot. If an additional focused laser beam perpendicular to the first one is adjusted so that the two spots overlap, and if the laser power is low enough to prevent considerable growth for only one beam, the deposition region is well defined by the intersection of the laser spots (Fig. 1). At this intersection, the absorbed energy is sufficient for a temperature rise that causes deposition from the gas phase. If the sample is moved slowly in any direction with a speed comparable to the growth rate of alumina, a structure with a complex shape can be directly written into free space.

Complex structures previously produced in this way are static, because every part is fixed directly or indirectly to the substrate. Here, we used this LCVD-based technique to build complex movable structures, such as a simple linear "micromotor," that are driven by thermal expansion forces caused by selective laser beam heating of structure parts. Devices of this kind can serve as micromechanical actuators.

The 3D structures described below were built on suitable substrates that were mounted inside a small reaction chamber on a turnable holder (Fig. 2). The effective laser power for the experiments was varied between 0.2 and 20 mW. The aluminum precursor trimethylamine alane [TMAA, $AlH_3{\cdot}N(CH_3)_3$] was pumped slowly through the chamber, which was maintained at a total pressure of ~1.6 mbar. For the production of aluminum oxide (Al_2O_3) rods, oxygen was used as an additional gas with a partial pressure of ~0.2 to 0.6 mbar. The dependence of structure growth on several parameters, such as oxygen partial pressure, has been described elsewhere (*10*).

Local laser heating of structure parts in a nonreactive atmosphere can produce thermal expansion effects that lead to slight bending of the parts. Because the linear expansion coefficient of aluminum is considerably higher than that of Al_2O_3, rods that were designed to expand and apply force on other structure parts were coated with aluminum. Because the thermal conductivity of aluminum is much higher than that of Al_2O_3, the coating provides a more uniform temperature distribution that prevents local heat peaks, which could damage the structure.

Lever constructions can be used to increase the distance of travel, and we built a set of microtweezers (Fig. 3) on the basis of this principle. With the use of a suitable lever, we were able to multiply the linear expansion of the laser-heated rod (~1 μm) by a factor of 20. The force the microtweezers can apply is currently limited by the flexibility of the lever that holds the lower tip. The applied force F can be calculated from

$$F = \frac{3\pi r^4 z E}{4L^3} \qquad (1)$$

where r is the radius of the lever, E is Young's modulus of alumina (5.2×10^{11} N m^{-2}), and L is the length of the lever (*11*). For r = 7 μm and L = 400 μm, and assuming a maximum bending of z = 5 μm, the force F is on the order of 0.1 mN—that is, more than 1000 times the weight of the tweezers. The maximum force may be further limited by the stability of the connection between the lever holder and the substrate.

The different thermal expansion coefficients of aluminum and alumina can also be used to cut rod connections to the substrate. When two parallel vertical aluminum-coated rods connected at the top are alternately laser-heated, the thermal strain leads to disconnection of the rod bases from the substrate. Freely movable structure parts can thus be manufactured by releasing them from the substrate after their shape has been defined by 3D laser direct writing.

Using the principles described above, we developed a simple linear micromotor with a maximum travel of ~100 μm (Fig. 4). The driving unit of the motor consists of three expandable rods that can be operated selectively. When the three rods are heated in a defined sequence, a closed movement of the horizontal rod R results (Fig. 5). The expansion of rods A and C bends the structure slightly to the left or to the right, respectively; hence, point P is moved to the left or to the right. When the laser beam is switched off, the shape of the structure re-

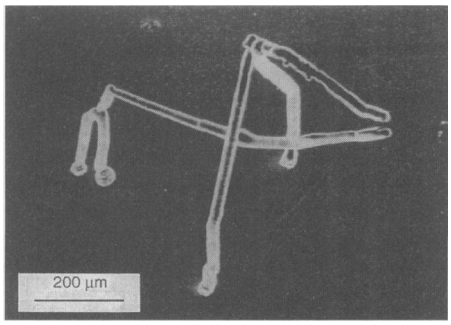

Fig. 3. Microtweezers fabricated by laser rapid prototyping. The tips of the tweezers (right) are moved together by the lifting of the lower lever, which is induced by laser heating and linear expansion of the right-hand rod in the pair of vertical rods (left). The long lever shifts the maximum travel to ~20 μm. The whole structure was fabricated within several minutes.

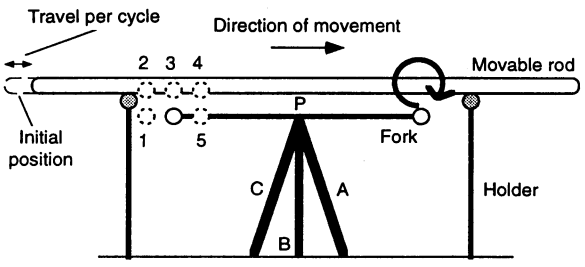

Fig. 5. Working scheme of the laser-driven linear micromotor (Fig. 4). A laser beam is scanned across the rods A, B, and C, causing a circular movement of the fork. During this cycle, the movable rod is lifted from the holders, moved to the right, and placed back on the holders.

turns to its initial state. Rod B is used for vertical movements; heating this rod results in a lift of point P. All travel distances are increased by lever constructions to maximum values of 20 μm at the lever end.

When a slightly defocused laser beam (diameter ~50 μm) is scanned from right to left over rods A, B, and C, the freely movable horizontal rod R is moved ~5 μm to the right and placed back on the holders. Each cycle consists of the following steps: (i) Heating of rod A moves the lever to the left. (ii) Heating of rods A and B moves the lever up; rod R is lifted from the holders H and rests on the lever fork F. (iii) Heating of only rod B results in the return of rod R to the middle horizontal position. (iv) Heating of rods B and C moves the lever further to the right. (v) Heating of only rod C lowers the lever; rod R is placed back on the holders H, but the position is shifted to the right relative to the initial state. (vi) Cessation of heating of rod C restores the horizontal beginning position of the lever. The motor is now ready for a new cycle. Repeating the cycle results in longer distances of travel (Fig. 6).

The working principle of the micromotor resembles the contraction of a muscle through the interaction of myosin and actin (*12*). The maximum force the motor can apply is limited in this simple model by the adhesion of the horizontal bar to the fork during the movement. This adhesion force, ~10 nN, is on the order of the weight of the bar. If this adhesion is increased (for example, by a rougher surface), much higher values of the force—in the micronewton range, as calculated for the microtweezers—can be expected.

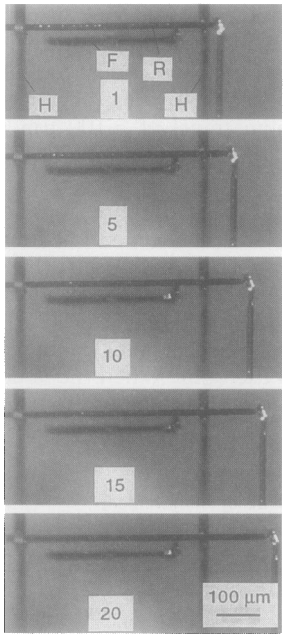

Fig. 6. Front view of the linear micromotor after 1, 5, 10, 15, and 20 cycles. The horizontal bar is moved ~100 μm to the right during 20 cycles (H, holders; F, fork; and R, rod).

The above examples suggest more complex applications for micromechanical devices fabricated by laser rapid prototyping from the gas phase. The one-step nature of the laser direct-write method makes structural evolution quick and easy, in contrast to mask-based processes. If focused laser light is used as the energy source, energy can easily be transferred to the moving structure; this would enable the creation of free "walking" devices with no mechanical connection to a battery or other energy source.

REFERENCES AND NOTES

1. T. M. Bloomstein and D. J. Ehrlich, *Appl. Phys. Lett.* **61**, 708 (1992); D. J. Ehrlich, *Appl. Surf. Sci.* **69**, 115 (1993).
2. F. T. Wallenberger, *Science* **267**, 1274 (1995).
3. D. Bäuerle, *Chemical Processing with Lasers* (Springer-Verlag, Heidelberg, 1987).
4. G. Leyendecker, D. Bäuerle, P. Geittner, H. Lydtin, *Appl. Phys. Lett.* **39**, 921 (1981).
5. D. Bäuerle, G. Leyendecker, D. Wagner, E. Bauser, Y. C. Lu, *Appl. Phys. A* **30**, 147 (1983).
6. F. T. Wallenberger and P. C. Nordine, *Science* **260**, 66 (1993).
7. P. C. Nordine, S. C. de la Veaux, F. T. Wallenberger, *Appl. Phys. A* **57**, 97 (1993).
8. F. T. Wallenberger and P. C. Nordine, *Mater. Lett.* **14**, 198 (1992).
9. M. Boman, H. Westberg, S. Johansson, J.-Å. Schweitz, *Proceedings of the 5th International Workshop on Micro Electro Mechanical Systems*, 4 to 7 February 1992, Travemünde, Germany (IEEE, Piscataway, NJ, 1992).
10. O. Lehmann and M. Stuke, *Mater. Lett.* **21**, 131 (1994).
11. *CRC Handbook of Chemistry and Physics* (CRC Press, Boca Raton, FL, ed. 61, 1981).
12. B. G. Levi, *Phys. Today* (April 1995), p. 17.

13. We thank K. Müller for expert technical assistance. Supported by Bundesministerium für Bildung, Wissenschaft, Forschung und Technologie grant 13N61597.

24 July 1995; accepted 16 October 1995

Defect Motion on an InP(110) Surface Observed with Noncontact Atomic Force Microscopy

Yasuhiro Sugawara, Masahiro Ohta, Hitoshi Ueyama, Seizo Morita

With an atomic force microscope operating in the noncontact mode in an ultrahigh vacuum, atomic-resolution imaging of the cleaved semi-insulating InP(110) surface has been achieved. By this method, atomic scale point defects and their motion were observed at room temperature, without the field-induced effects associated with scanning tunneling microscopy.

The ability to resolve individual atoms over a wide area makes the scanning tunneling microscope (STM) an excellent tool for studying the migration of atoms or defects. However, in all real-time STM experiments of surface dynamics processes, there is a high probability that the motion is nonthermal and is instead affected by the electric field or tunneling current; that is, the migration of the atoms or defects is the result of an excitation by the electric field of the biased tip or an energy injection by the tunneling current. It is well known that manipulation of single atoms is possible with the STM (*1*). Furthermore, STM tip–induced motion of the atoms or defects can exceed the thermal motion at room temperature (*2, 3*). To investigate surface dynamics processes related to thermally induced motion of atoms or defects, one must remove tip-induced nonthermal motion.

The atomic force microscope (AFM) (*4*) is an alternative tool for high-resolution imaging. When operating in noncontact mode, it is expected to be free of such nonthermal effects and therefore to be effective for observing thermally induced motion in real time, because its operation is based on weak interactions attributable to attractive forces, rather than the electric field utilized in the STM. So far, the lateral resolution of noncontact ultrahigh-vacuum (UHV) AFM has been insufficient because of technical difficulties in measuring the weak distance dependence of the attractive forces between tip and sample, which have the high signal-to-noise ratio of the force measurements. Recently, the adatoms of the Si(111) 7×7 reconstructed surface were resolved locally by AFM, but stable imaging was not achieved (*5*). Furthermore, the distances between the adatoms and the corrugation heights with corner holes on the Si(111) 7×7 reconstructed surface are relatively large compared with those of other semiconductor surfaces. Continuing technical improvements increasing the lateral resolution of noncontact UHV AFM are required.

In this report, we present noncontact UHV-AFM images with atomic resolution for the semi-insulating InP(110) surface. Atomic scale point defects have been ob-

Department of Physics, Faculty of Science, Hiroshima University, 1-3-1 Kagamiyama, Higashi-Hiroshima, Hiroshima 739, Japan.